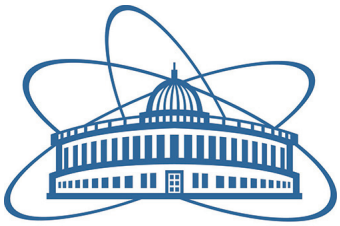


# Production and spectroscopic investigation of new neutron-rich isotopes near the neutron N=126 shell closure using the multi-nucleon transfer reactions

**By**

**Abdelrhman Hussam**

Physics Department, Faculty of Science, Cairo University, Giza, Egypt

**Supervisor**

**Mr Viacheslav Vedeneev**

Flerov Laboratory of Nuclear Reactions,Dubna, Russia

Wave 5 Final Report

Joint Institute For Nuclear Research, Dubna, Russia

October 23, 2021

# Contents

# Abstract

The MASHA (Mass Analyzer of Super Heavy Atoms) was created to produce and mass identify super-heavy nuclei near shell closure ($N = 126$) using the solid ISOL method, which is commonly employed in the mass analysis of short-lived isotopes and separates them from the principal ion beam in an on-line manner. MASHA enables us to determine the mass-to-charge ratios of SHE isotopes while also detecting their decays and spontaneous fission. By better understanding these factors, topics such as "island of stability" can be explored. The isotope separation on line method was employed in this study. The MASHA system was used to study the products of the fusion nuclear events $^{40}Ar+^{148}Sm$, $^{40}Ar+^{166}Er$, and the multi-nucleon transfer process $^{48}Ca+^{242}Pu$, which found and examined neutron-deficient mercury and radon isotopes through their alpha decay chains.

# 1 Introduction

The study of super-heavy nuclei is one of the most important studies in nuclear physics, which is constantly being developed. It aims to describe the nuclear interaction and the structure of the envelope, which indicates their presence.

Research about physical properties of super-heavy elements (SHE), such as decay energy and modes, mass, and half-life has stimulated the design and construction of the Mass Analyser of Super Heavy Atoms (MASHA) at one of the beam outs of U-400M cyclotron based in Flerov Laboratory of Nuclear Reactions (FLNR) at Joint Institute for Nuclear Research (JINR), Dubna, Russia.

The mass analyzer's unique potential can be attributed to its ability to concurrently measure the masses of produced super-heavy element isotopes while also detecting their decays and/or spontaneous fission. Another application for the mass-separator MASHA is the study of neutron-rich nuclei at the N=126 neutron shell. These nuclei will be created in multi-nucleon transfer processes with target-like nuclei separated by mass-to-charge ratio. In this type of reaction, the target and catcher systems will be employed, with the target material being solved in the catcher material utilising the Isotope Separation On-Line (ISOL) method. The reaction processes studied in this project were:

$$^{40}Ar + ^{148}Sm \quad \rightarrow \quad ^{188-xn}Hg + xn$$

$$^{40}Ar + ^{166}Sm \quad \rightarrow \quad ^{206-xn}Hg + xn$$

$$^{48}Ca + ^{242}Pu$$

As can be seen, the first two reactions are fusion reactions with neutron evaporation residues, while the last is a multi-nucleon transfer reaction, where neutron-deficient mercury and radon isotopes were identified and studied through their $\alpha$ decay chains.

# 2 Experimental Setup

## 2.1 MASHA Setup

The installation main parts are hot catcher; an ion source based on the electron cyclotron resonance (ECR); a magneto optical analyzer (mass spectrometer) composed of four dipole magnets ($D_1$, $D_2$, $D_{3a}$, and $D_{3b}$), three quadrupole lenses ($Q_1$–$Q_3$), and two sextupole lenses ($S_1$, $S_2$); and a detection system located in the spectrometer's focal plane are shown in Figure [2.1] .The mass spectrometer's ion optical system was thoroughly examined in [3,4]. The separate units of the setup are described in this section, as well as the results of measurements of the important separator features.

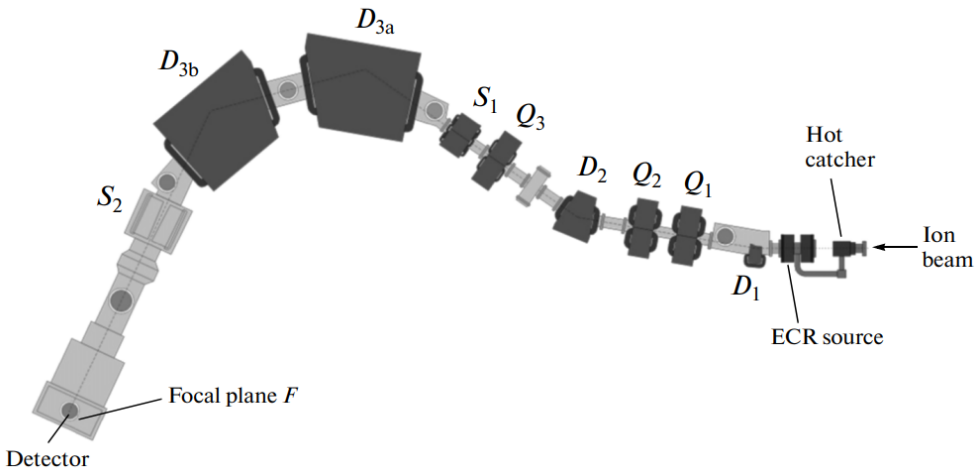


Figure 2.1: Schematic diagram of the MASHA mass separator: ($D_1$, $D_2$, $D_{3a}$), and $D_{3b}$) dipole magnets, ($Q_1, Q_2, Q_3$) quadrupole lenses, and ($S_1$, $S_2$) sextupole lenses. The detection system is in focal plane F of the separator.

### 2.1.1 Ion Source

For ionizing atoms of nuclear reaction products, an ion source based on the ECR (the ECR source) with a microwave oscillator frequency of $2.45 GHz$ was used Figure[2.2]. Provided a description of

this source as well as its characteristics. Atoms are ionized to charge state $Q = +1$ in the ECR, then accelerated with the three electrode system and assembled into a beam, which is then separated by the mass spectrometer's magneto optical system. The ECR source aids in the generation of ion currents that contain about 100% of singly ionized atoms, and the ionisation efficiency of noble gases is as high as 90%. The power and frequency of microwave radiation, as well as the buffer gas pressure in the ionizer chamber, were used to optimize the ECR source's working modes. A controlled piezoelectric valve was utilised to manage the pressure of helium, which was used as a buffer gas. At a helium pressure of $(1-2)10^{-5}$ *mbar* and a microwave oscillator power of 30 $W$, the source's optimum characteristics were established.

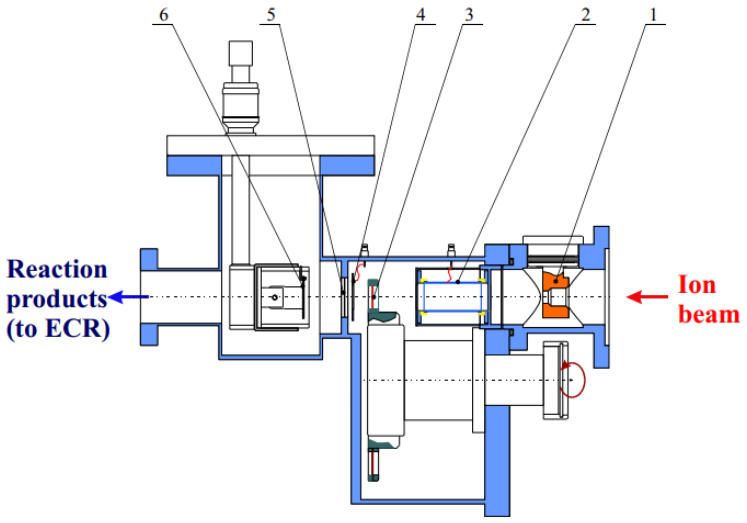


Figure 2.2: Schematic overview of the target-hot catcher system. Here: 1 – diaphragm; 2 – pick-up sensor; 3 – target on the wheel; 4 – electron emission beam monitor; 5 – separating foil; 6 – hot catcher.

### 2.1.2 A Target Assembly and a Hot Catcher

A hot catcher was used to introduce products of full fusion events into the ECR source in the first tests targeted at detecting the masses of isotopes of the $112^{th}$ and $114^{th}$ elements. The hot catcher is physically a part of the target assembly depicted in Figure [2.3]. The primary beam of heavy ions goes through the diagnostic system, which consists of a split type aperture of the electrostatic induction sensor and a Faraday cup, before striking the target. Each of the four sectors of the split aperture measures the fraction of the beam current that does not fall into the aperture's hole. This system allows

you to regulate the position of the beam in relation to the ion guide. The induction sensor is a stainless steel tube that is set in place on an electrically isolated frame past the split aperture downstream of the beam and is used to monitor the current during the experiment.

At a distance of 70*mm* in front of the target, the Faraday cup is set in place on the rotational vacuum tight feedthrough. Nuclear reaction products escape from the target, pass through the separating foil, and are trapped in a graphite absorber heated to $1500 - 2000\ K$. The products diffuse as atoms from the graphite absorber to the vacuum volume of the hot catcher and then to the ECR source through the pipeline. In the hot catcher, an absorber material made of heat expanded graphite foil with a density of $1 g/cm^3$ and a thickness of 0.6*mm* is utilised. The graphite absorber is designed like a 30*mm* diameter disc that is placed 30*mm* behind the target.The graphite absorber heats directly from current of $150 - 170\ A$, heats the absorber. An IR pyrometer was used to calibrate the temperature of the

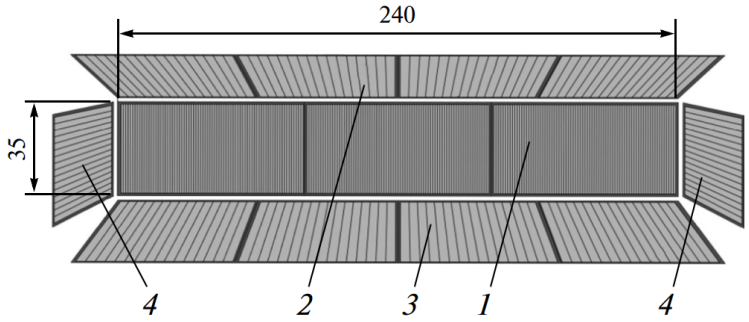


Figure 2.3: Frontal part (192 strips), (2) top part (64 strips), (3) bottom part (64 strips), and (4) side parts (16 strips in each).

graphite absorber, which had been put outside the vacuum chamber of the target assembly before the beam tests. Radiation from the heated graphite, which emerged through the sapphire window, was detected by the pyrometer. Because it was unable to monitor the temperature during the experiments due to the target assembly's arrangement, the temperature of the graphite absorber was determined during the measurements by the heater current.

### 2.1.3 Detection and Control System

To detect decays of nuclear reaction products, a well-type silicon detector is mounted in the focus plane of the mass spectrometer. The 192 strips make up the plane of the frontal detector component, which is

positioned normal to the beam direction. Each of the side detectors is divided into 64 and 16 strips. The detectors have a conventional operating bias of ˘40$V$ and a 30$keV$ energy resolution for particles from a $^{226}Ra$ source. The detector assembly's stated design allows it to detect no less than 90% of particles emitted in a single nuclear decay at the detector's frontal section. Each strip of the silicon detector's signals is read out separately. The application displays one-dimensional energy spectra for each strip as well as two-dimensional spectra for each crystal's energy dependency on strip number.

## 2.2 Experimental Technique

MASHA was constructed at one of the beam outs of $U-400M$ cyclotron in order to conduct online measurements of the physical properties of super-heavy elements.The target was bombarded by beam of $^{48}Ca$ with energy $E_{beam} = 7.3MeV/n$. The beam is stopped in the graphite catcher heated up to 1800$K$. Atoms diffuse from the graphite volume and, move along the vacuum pipe and reach the ECR ion source discharge chamber where they are ionized.

Faraday cup allows beam intensity control or target protection by periodically interrupting the beam.The separation efficiency and time were measured for Hg isotopes due to their similarity with element $Z = 112$ and $Z = 114$ [1,2]. $\alpha$ radioactive isotopes were obtained in the fusion reaction. $\alpha$ decay energy of the fusion products was measured as a function of the strip number.

$$^{40}Ar + ^{144}Sm \quad \rightarrow \quad ^{184-xn}Hg + xn$$

The full separation efficiency for the short-lived mercury isotopes was 7% and the separation time was 1.8$s$. $Rn$ was obtained in the $^{40}Ar + ^{166}Er$ reaction and in the multi-nucleon transfer reaction $^{48}Ca + ^{242}Pu$, which also has a high cross section and used as a homologue of $Cn$.

# 3 Result and Discussion

In this chapter we will represent and analyze the results of the nuclear reactions taken from MASHA.

## 3.1 Reaction $^{40}Ar + ^{148}Sm$

From Figure 3.1[a,b,d], we can see the energy at which the elements of mercury appeared and the energy of appearance of the elements of *Pt* after decay alpha.In Figure 3.1[c,e,f]. It is clear that each of 182, 184 and 185 $Hg$ does not show daughters after alpha decay, but only shows the peak of the parents.The experimental data were compared with the theoretical studies of the energies of the elements that were observed, and these results are summarized in Table [3.1].

Table 3.1: comparison between experimental and theoretical energy of the nuclei.

| Nucleus | $T_{1/2}\ (Sec)$ | $Energy\ Exp\ (keV)$ | $Energy\ Theo\ (keV)$ | %Δ |
|---|---|---|---|---|
| $^{180}Hg$ | 2.85 | 6120 | 6119 | 0.01 |
| $^{176}Pt$ | 6.3 | 5750 | 5753 | 0.05 |
| $^{181}Hg$ | 3.54 | 6000 | 6006 | 0.1 |
| $^{177}Pt$ | 11 | 5500 | 5517 | 0.3 |
| $^{182}Hg$ | 10.82 | 5860 | 5867 | 0.11 |
| $^{183}Hg$ | 9.4 | 5890 | 5904 | 0.23 |
| $^{184}Hg$ | 30.9 | 5530 | 5535 | 0.09 |
| $^{185}Hg$ | 49.1 | 5650 | 5653 | 0.05 |

We can also see the theoretical results for the half life time of these nuclei.It is noticeable in Table [3.1], that the experimental and theoretical results are very close, and this indicates the accuracy of the mass analyzer MASHA, and we can also consider the difference in the energy value in the experimental and theoretical results.The alpha decay energy and strip number in the frontal part of the silicon detector placed in the focal plane are illustrated in figure[3.2]. The magnetic system and detector have excellent resolution, distinguishing the various isotopes both in mass and energy.

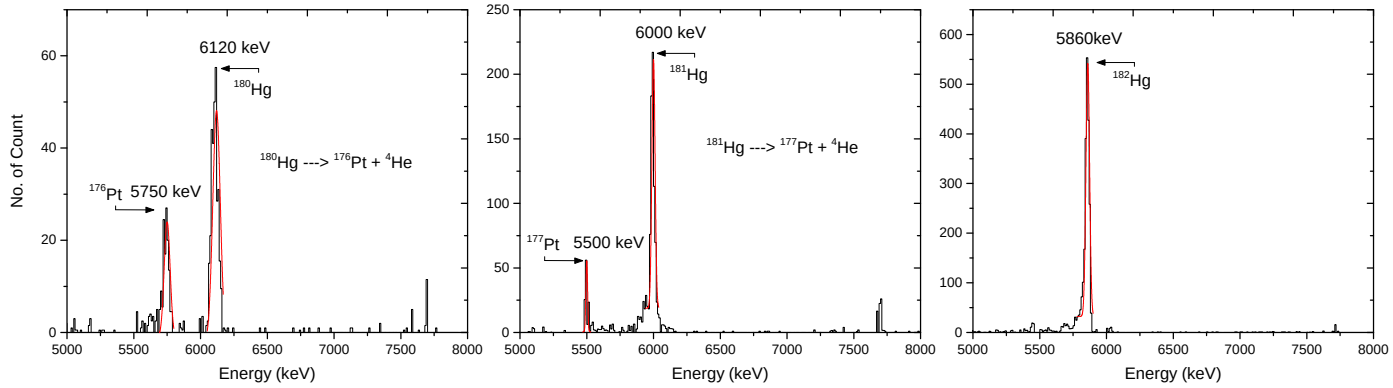


(a) (b) (c)

Figure 3.1

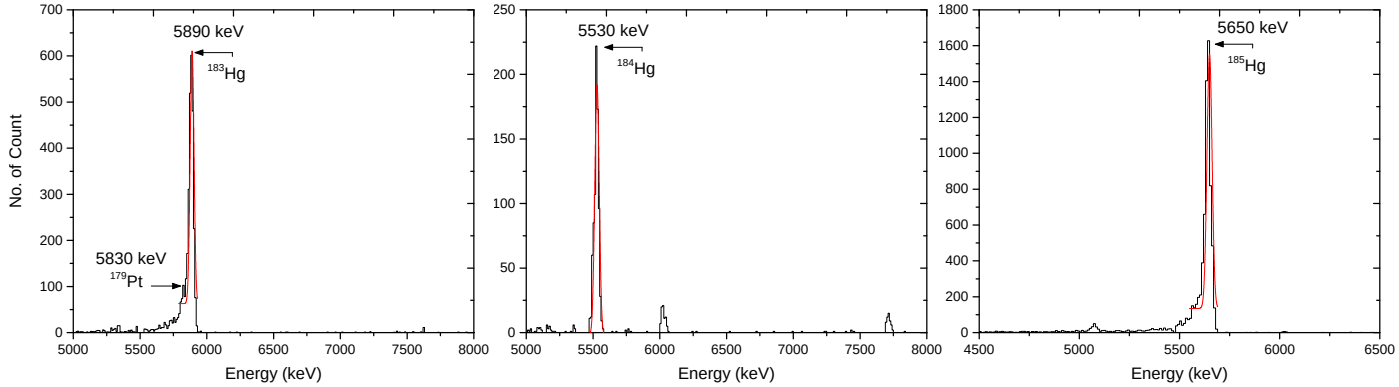


(a) (b) (c)

Figure 3.2

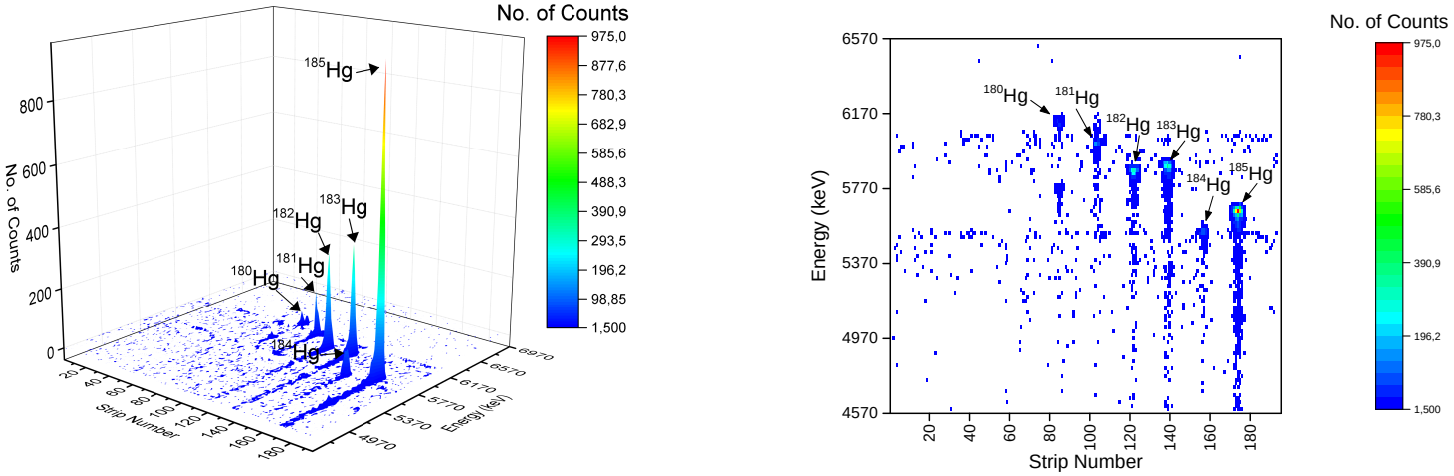


(a) (b)

Figure 3.3

## 3.2 Reaction $^{40}Ar + ^{166}Er$

Table [3.2] shows a contrast between the theoretical and practical values of the energy values of the detected nuclei, as well as the values of the half life time in different units. We can note the high differences between the values of the experimental and theoretical compared to the previous interaction. In Figure [3.4,3.5] the peaks are clearly shown whether they are Rn or Po nuclei. The decays which we can extract are,

$$
\begin{aligned}
^{201}Rn &\rightarrow {}^{197}Po + {}^{4}He \\
^{202}Rn &\rightarrow {}^{198}Po + {}^{4}He \\
^{203}Rn &\rightarrow {}^{199}Po + {}^{4}He \\
^{204}Rn &\rightarrow {}^{200}Po + {}^{4}He \\
^{205}Rn &\rightarrow {}^{201}Po + {}^{4}He
\end{aligned}
$$

As seen in Figure [3.4,3.5], there are Small peaks of the same isotope appear, and looking at Table [3.2], we find that they have theoretical values

Table 3.2: comparison between experimental and theoretical energy of the nuclei.

| Nucleus | $T_{1/2}$ | $Energy\ Exp\ (keV)$ | $Energy\ Theo\ (keV)$ | $\%\Delta$ |
|---|---|---|---|---|
| $^{201}Rn$ | 7.1 S | 6780 | 6773 | 0.1 |
| $^{197}Po$ | 53.6 S | 6380 | 6383.4 | 0.05 |
| $^{197}Po$ | 53.6 S | 6280 | 6281 | 0.01 |
| $^{202}Rn$ | 10.0 S | 6630 | 6639.5 | 0.14 |
| $^{198}Po$ | 1.77 M | 6180 | 6182 | 0.03 |
| $^{203}Rn$ | 45 S | 6550 | 6549 | 0.01 |
| $^{199}Po$ | 5.48 M | 6060 | 6059 | 0.01 |
| $^{199}Po$ | 5.48 M | 5960 | 5952 | 0.13 |
| $^{204}Rn$ | 1.2 M | 6400 | 6418.9 | 0.29 |
| $^{200}Po$ | 11.5 M | 5880 | 5861.9 | 0.3 |
| $^{205}Rn$ | 170 S | 6270 | 6268 | 0.03 |
| $^{201}Po$ | 15.3 M | 5910 | 5786 | 2.0 |

And as in the previous reaction, Figure [3.6] shows The alpha decay energy and strip number in the frontal part of the silicon detector placed in the focal plane.

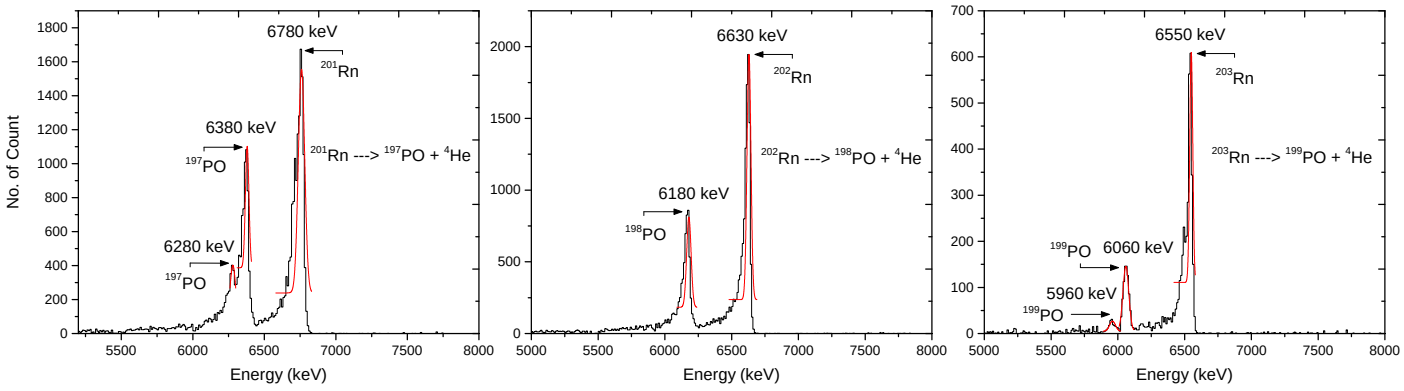


(a) (b) (c)

Figure 3.4

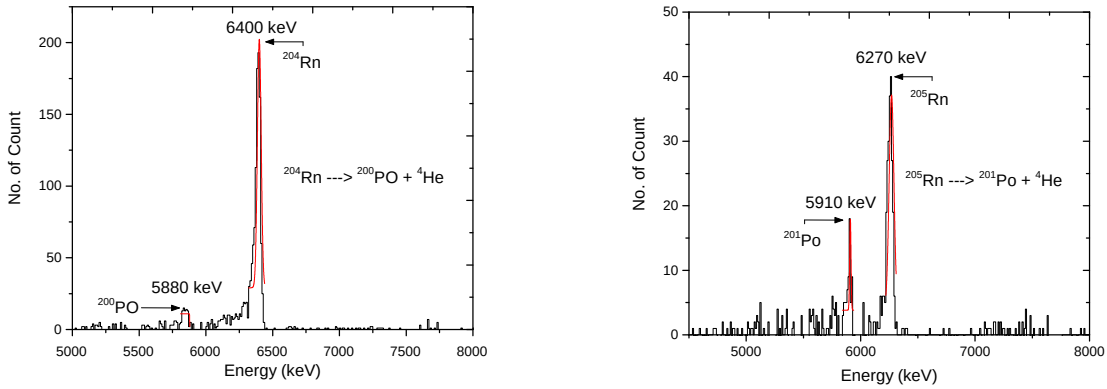


(a) (b)

Figure 3.5

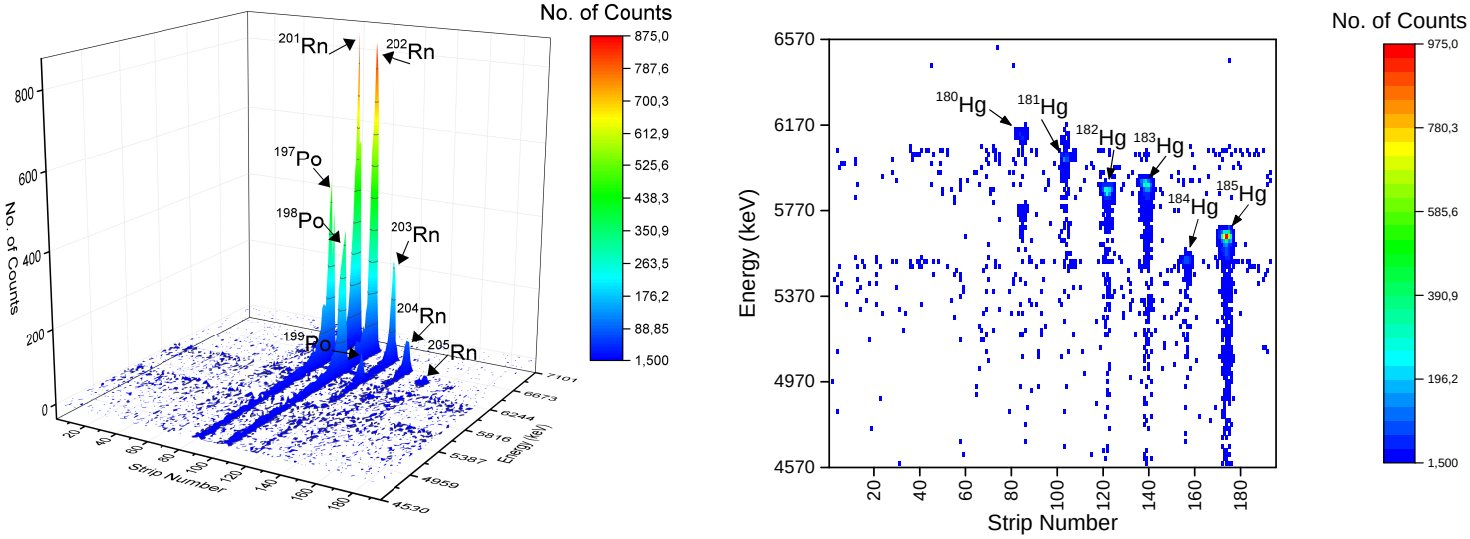


(a) (b)

Figure 3.6

## 3.3 Reaction $^{48}Ca+^{242}Pu$

Table [3.3] shows a contrast between the theoretical and experimental values of the energy of the detected nuclei, as well as the values of the half life time in different units. We can note the high differences between the values of the experimental and theoretical compared to the previous interactions, $^{40}Ar+^{148}Sm$ and $^{40}Ar+^{166}Er$. In Figure [3.7] the peaks are clearly shown whether they are Rn, Po or Bi nuclei. The decays which we can extract are,

$$^{218}Rn \rightarrow {}^{214}Po+{}^{4}He$$
$$^{219}Rn \rightarrow {}^{215}Po+{}^{4}He$$

As seen in Figure [3.7.b,3.7.c], there are clearly peaks of the same isotope appear, and looking at Table [3.3], we find that they have theoretical values.

Table 3.3: comparison between experimental and theoretical energy of the nuclei.

| Nucleus | $T_{1/2}$ | $Energy\ Exp\ (keV)$ | $Energy\ Theo\ (keV)$ | $\%\Delta$ |
|---|---|---|---|---|
| $^{212}Rn$ | 23.9 M | 6250 | 6264 | 0.22 |
| $^{218}Rn$ | 35 MS | 7110 | 7129.2 | 0.27 |
| $^{214}Po$ | 164.3 M | 6590 | 6609.8 | 0.3 |
| $^{214}Po$ | 164.3 M | 7660 | 7686.82 | 0.35 |
| $^{210}Po$ | 138.376 D | 5280 | 5304.33 | 0.46 |
| $^{210}Bi$ | 5.013 D | 4120 | 4100 | 0.48 |
| $^{215}Po$ | 1.781 MS | 7360 | 7386.1 | 0.35 |
| $^{219}Rn$ | 3.96 S | 6790 | 6819.1 | 0.42 |
| $^{219}Po$ | 3.96 S | 6600 | 6552.6 | 0.71 |

And as in the previous reaction, Figure [3.8] shows The alpha decay energy and strip number in the frontal part of the silicon detector placed in the focal plane.

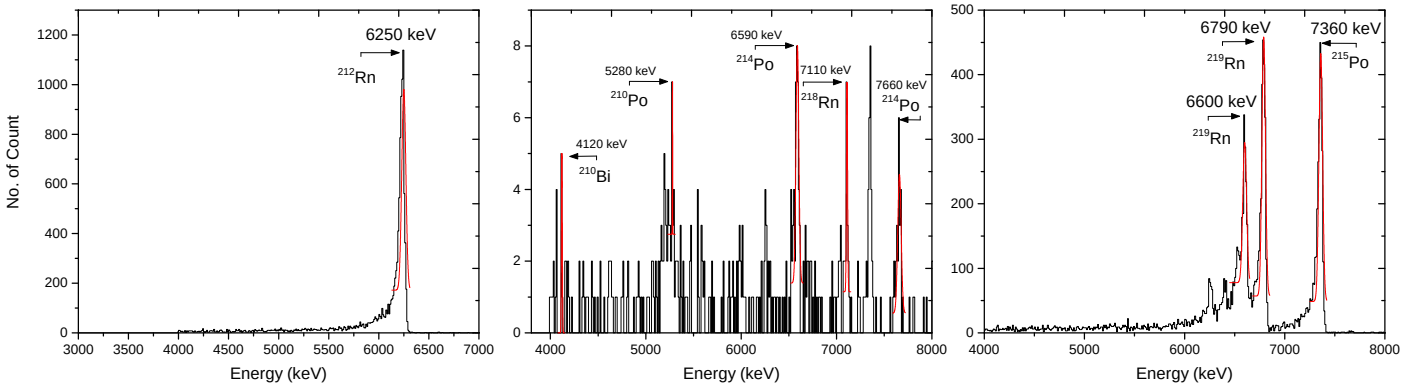


(a) (b) (c)

Figure 3.7

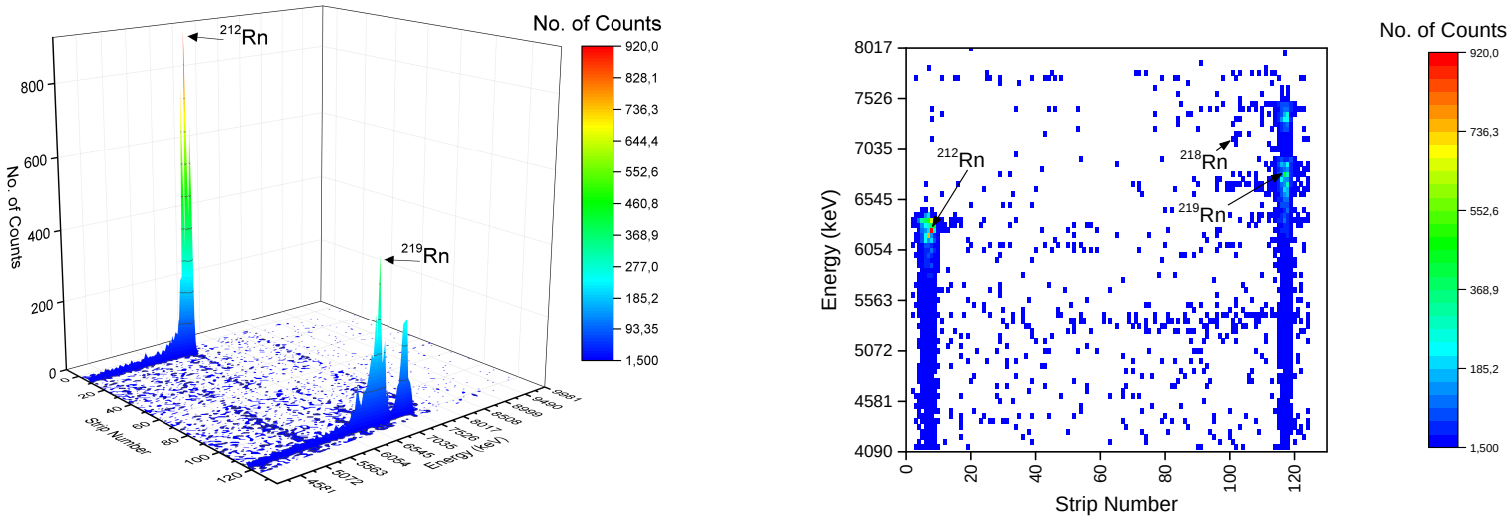


(a) (b)

Figure 3.8

# Conclusions

The existence of the "Island of the Stability," which is a predicted group of isotopes of super-heavy elements that may have far longer half-lives than known isotopes of these elements, is revealed by a detailed examination of super-heavy elements. During the experiment, the energy spectra of the alpha decay were measured at the focal plane using the silicon detection system.

By analyzing interaction data. We were able to identify the nuclei of mercury and radon and compare their experimental results with the theoretical results that have been studied. The comparison showed closeness in the experimental and theoretical results for mercury nuclei, but in the case of radon nuclei, there was a clear difference between the results.

# Acknowledgments

I would like to thank Joint Institute for Nuclear Research for this great opportunity, which is based on mixing with real projects and dealing with them to gain experience.

# Bibliography

[1] S. N. Dmitriev, Y. T. Oganessyan, V. K. Utyonkov, S. V. Shishkin, A. V. Yeremin, Y. V. Lobanov, Y. S. Tsyganov, V. I. Chepygin, E. A. Sokol, G. K. Vostokin, *et al.*, "Chemical identification of dubnium as a decay product of element 115 produced in the reaction 48ca+ 243am," *Mendeleev Communications*, vol. 15, no. 1, pp. 1–4, 2005.

[2] R. Eichler, N. Aksenov, A. Belozerov, G. Bozhikov, V. Chepigin, S. Dmitriev, R. Dressler, H. Gäggeler, V. Gorshkov, F. Haenssler, *et al.*, "Chemical characterization of element 112," *Nature*, vol. 447, no. 7140, pp. 72–75, 2007.

[3] V. Y. Vedeneev, A. Rodin, L. Krupa, A. Belozerov, E. Chernysheva, S. Dmitriev, A. Gulyaev, A. Gulyaeva, D. Kamas, J. Kliman, *et al.*, "The current status of the masha setup," *Hyperfine Interactions*, vol. 238, no. 1, p. 19, 2017.

[4] A. Rodin, A. Belozerov, D. Vanin, V. Y. Vedeneyev, A. Gulyaev, A. Gulyaeva, S. Dmitriev, M. Itkis, J. Kliman, N. Kondratiev, *et al.*, "Masha separator on the heavy ion beam for determining masses and nuclear physical properties of isotopes of heavy and superheavy elements," *Instruments and Experimental Techniques*, vol. 57, no. 4, pp. 386–393, 2014.